applied sciences

MDPI

Article

Study on Heating Performance and Flexural Strength Properties of Electrically Conductive Mortar

Dong-Ju Seo [1], You-Jae Lee [1], Beom-Gyun Choi [1], Jong-Gun Park [2,*] and Gwang-Hee Heo [3]

[1] School of Disaster and Safety Engineering, Konyang University, 121, Daehak-ro, Nonsan-si 32992, Republic of Korea; ws9500@naver.com (D.-J.S.); leelou@hanmail.net (Y.-J.L.); chlqjarbs@naver.com (B.-G.C.)
[2] Public Safety Research Center (PSRC), Konyang University, 121, Daehak-ro, Nonsan-si 32992, Republic of Korea
[3] Department of International Civil and Plant Engineering, Konyang University, 121, Daehak-ro, Nonsan-si 32992, Republic of Korea; heo@konyang.ac.kr
* Correspondence: park2630@konyang.ac.kr

Abstract: The use of electrically conductive mortar (ECM) is a relatively new construction material technology developed to obtain high conductivity and mechanical strength. This study presents an experimental investigation on the heating performance and flexural strength properties of ECM mixed with carbon fiber (CF) and steel fiber (SF), which are conductive fibers. Furthermore, the internal microstructure of the ECM was analyzed with a scanning electron microscope (SEM) and thermogravimetric analysis was carried out using a thermogravimetric analyzer (TGA) device. The results of the experiment showed that the incorporation of SF had little effect on heating performance. In the case of CF, however, it was found that as the fiber contents and applied voltages increased, the heating performance increased. In particular, the maximum heating temperature of the ECM-CF125 specimen was 145.1 °C at an applied voltage of 30 V and an electrode spacing of 40 mm, which was about 7.3 times higher than the initial temperature (20 °C). In addition, the flexural strength of ECM mixed with SF was higher than that of plain mortar (PM), whereas the ECM-CF125 specimen showed a greater tendency to significantly decrease. It was confirmed that the hydration products and internal microstructures of the specimens were unaffected by repetitive electrical heating, and the ECM maintained stable electrical conductivity.

Keywords: electrically conductive mortar (ECM); carbon fiber (CF); steel fiber (SF); heating performance; flexural strength

check for updates

Citation: Seo, D.-J.; Lee, Y.-J.; Choi, B.-G.; Park, J.-G.; Heo, G.-H. Study on Heating Performance and Flexural Strength Properties of Electrically Conductive Mortar. *Appl. Sci.* **2023**, *13*, 9903. https://doi.org/10.3390/app13179903

Academic Editor: Asterios Bakolas

Received: 19 July 2023
Revised: 23 August 2023
Accepted: 28 August 2023
Published: 1 September 2023

Copyright: © 2023 by the authors. Licensee MDPI, Basel, Switzerland. This article is an open access article distributed under the terms and conditions of the Creative Commons Attribution (CC BY) license (https://creativecommons.org/licenses/by/4.0/).

1. Introduction

For the development of multifunctional fiber-reinforced cement-based composites demanded by today's market, many studies have been conducted on electrically conductive heating cement composites and their mechanical properties [1–5]. In particular, studies on cement-based composite materials incorporating conductive materials and existing cement-based composite materials known as insulators have been actively conducted. It is well known to many previous researchers that the better the conductivity, the better the heating performance [6–9].

Cement is the most widely used construction material in the fields of civil engineering and buildings due to its abundant resources, good environmental adaptability, low cost and high compressive strength [10,11]. It is itself an electrical insulating material. Specifically, its electrical resistivity lies at the boundary between insulators and poor semiconductors [12,13]. Cement-based composites include electrically conductive cement paste (cement and water only) [14,15], electrically conductive mortar (with cement, water and fine aggregate) [16,17], electrically conductive concrete (with cement, water and fine and coarse aggregates) [18,19] and other electrically conductive composites [20,21].

Traffic accidents and human casualties due to road surface icing in winter are continuously occurring. In cold regions, reduced mobilization capacity of transportation networks often occurs during the winter season because of delays associated with ice and snow accumulation. In general, electrically conductive materials are classified into carbon-based materials and metal-based materials. Carbon fibers, steel fibers, graphite, carbon black, steel shavings, carbon nanotubes, carbon nanofibers, nickel particles, iron powder and expanded graphite are some examples of conductive materials utilized so far. In recent years, electrically conductive fiber-reinforced cement-based composites have become part of a very attractive research direction. Adding conductive fibers such as carbon fiber (CF) and steel fiber (SF) to cement-based composites can not only improve mechanical properties but also enhance the electrical and heating properties of cement-based composites [22–25]. Therefore, when a voltage is applied to conductive cement composites using embedded electrodes, heat is generated by the Joule heating principle. Since the generated heat efficiently converts electrical energy to thermal energy, it can be applied to various products. However, current research is limited to the electrical properties of hardened fiber-reinforced cement composites, whereas the electrical and heating performances of fresh fiber-reinforced cement composites are less studied. This type of cement-based conductive composite is particularly suitable for snow removal and deicing of pavements such as bridge decks and tunnel entrances and exits, airport runways, sidewalks, driveways and parking garages, etc. and is also fit for heating materials such as floor tiles and partition walls of buildings [26–31].

SF has excellent physical properties such as high tensile strength and elongation, but strength reduction and corrosion occur in an alkaline environment, whereas CF has excellent tensile strength and physical performance, but is limitedly used due to appropriate dispersion and high cost. However, CF is also very useful in enhancing both the mechanical and electrical properties of cement composites. In particular, the incorporation of CF can significantly reduce the electrical resistivity of cement-based composites while simultaneously enhancing the flexural performance (flexural strength and toughness). When an electrical potential (voltage) is applied to electrodes embedded in a cement-based composite mixed with CF, a conductive path through which charges can move is formed by CF, and heat is generated due to inherent resistance. The incorporation of CF was found to contribute to improving flexural performance while greatly reducing electrical resistivity [32–34]. In the case of CF, which has excellent conductivity due to its low electrical resistivity among carbon-based materials, it is imperative to consider its heating properties according to the variation in the amount of supplied current. However, information regarding research and development using CF as a heating element in cement-based composites is still somewhat lacking.

In order for a construction material to be applied to actual sites for snow melting and deicing of pavements, not only electrical and heating performance but also flexural strength of design must satisfy a certain level at the same time. In the Republic of Korea, the standard specification for road construction (cement concrete pavement work) stipulates that "the design standard flexural strength of cement concrete for pavement should be 4.5 MPa or more" [35]. Accordingly, the ultimate goal of this study is to develop an electrically conductive mortar (ECM) that can simultaneously satisfy the heating performance and flexural strength requirements of mortar mixed with conductive fibers. Its purpose is to provide basic data for field application as an eco-friendly construction material for snow melting as well as deicing on the surface of pavements in the future.

Therefore, this study purports to fabricate ECM mixed with conductive fibers such as CF and SF and to investigate the effects on the heating performance and flexural strength properties. To this end, fiber volume fractions were varied from 0.25% to 1.25% at 0.25% intervals to prepare specimens. Then, their performance was compared and reviewed with plain mortar (PM). At the same time, the surface temperature of each specimen was measured using an infrared thermal camera (T630sc, FLIR, Wilsonville, USA) at various applied voltages (DC 10 V, 20 V, 30 V) and different electrode spacings (40 mm, 120 mm). Furthermore, in order to examine the internal microstructure of the ECM under repetitive

electrical heating, images analysis using a scanning electron microscope (SEM) as well as thermogravimetric analysis using a thermogravimetric analyzer (TGA) were performed.

2. Experimental Investigation

2.1. Experimental Plan

In an effort to investigate the effect of ECM on heating performance and flexural strength properties in this study, the fiber content was selected at a total of 5 levels, that is, 0.25, 0.5, 0.75, 1.0 and 1.25% by volume. We planned to perform the experiments with parameters of various applied voltages (DC 10 V, 20 V, 30 V) and different electrode spacings (40 mm, 120 mm) and also planned, at the same time, to measure the surface temperature of each specimen using an infrared thermal camera (FLIR T630sc, Wilsonville, OR, USA). A flexural test was planned to review the flexural strength of PM and ECM. In addition, we planned to implement SEM images and TGA analysis to examine the internal microstructure properties of the ECM under repetitive electrical heating. Table 1 shows the variables and levels for the heating performance experiment considered in this study.

Table 1. Experimental plan of heating performance considered in this study.

Factors	Levels
Fiber volume fractions (%)	0.25, 0.5, 0.75, 1.0, 1.25
Applied voltages (V)	DC 10, 20, 30
Electrodes spacings (mm)	40, 120
Measurement device	Infrared thermal camera (FLIR T630sc) Universal testing machine (UTM) SEM observation TGA analysis

2.2. Materials

The cement used in this study was Type I ordinary Portland cement (OPC) from H Company (Sokcho, Republic of Korea). In this study, standard sand in Hyangho-ri, Jumunjin-eup, Gangwon-do, was used to make homogeneous mortar. Standard sand is a material containing natural round particles and 98% or more silicon dioxide (SiO_2) as specified by KSL ISO 679 [36], with an average particle diameter of 0.5 mm or less. The specific gravity and water absorption of the fine aggregate in the dry saturated state were 2.65 and 0.1%, respectively. The physical properties and particle size of the fine aggregate are shown in Table 2. A polycarboxylate-type superplasticizer (SP), a domestic product (Sika Korea Central, Co., Ltd., Gunsan, Republic of Korea), was used as chemical admixture for fluidity control of ECM. The used dosage of SP admixture was based on the mass of cement, an appropriate amount that satisfies the required ECM fluidity within the range of 0.5~1.0%. The SF used in this study is a hook-style product of bundle type with a length of 30 mm and a diameter of 0.5 mm produced by K company in the Republic of Korea, and the CF is a product (T700SC) of D company in Japan, with a length of 6 mm and a diameter of 7 μm. In the case of CF, a polyacrylonitrile (PAN)-based material having a carbon content of 92% or more, an electrical resistivity of 1.6×10^{-3} Ω.cm and a thermal conductivity of 6.4 W/m·K was used. The physical and mechanical properties of the conductive CF and SF used in this study are shown in Table 3, and these were provided by the manufacturers.

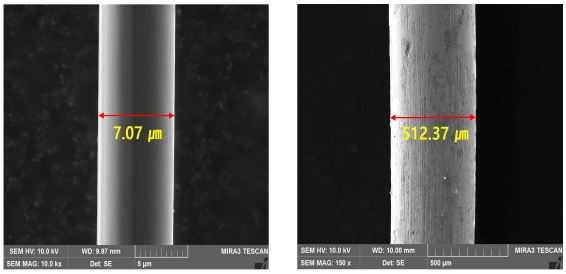
Table 2. Physical properties and grain size of fine aggregate.

Size (mm)	Unit Weight (kgf/m^3)	Density (g/cm^3)	Absorption (%)	Amount of Passing 0.3 mm Sieve (%)	Fineness Modulus (FM)
2≤	1490	2.65	0.1	3.0	2.40

Table 3. Properties of conductive fibers used in this study.

Fiber Type	Average Length, l (mm)	Average Diameters, d (mm)	Aspect Ratio (l/d)	Density (kg/m^3)	Tensile Strength (MPa)	Elastic Modulus (GPa)	Electrical Resistivity (Ω·cm)
CF	6	0.007	857	1800	4900	230	1.6×10^{-3}
SF	30	0.5	60	7850	1100	>210	1.3×10^{-4}

Figure 1 is a picture of conductive CF and SF enlarged with SEM imaging. Figure 1a shows a SEM picture of the surface shape of CF taken at a magnification of 10,000 times. The diameter of the CF is about 7.07 μm and the surface is very smooth, showing very poor interfacial adhesion with the cement matrix. On the other hand, Figure 1b shows a SEM picture of the surface shape of SF taken at a magnification of 150 times. The diameter of SF is about 512.37 μm and the surface looks somewhat rough, presumably forming a surface texture that is advantageous for interfacial adhesion to the cement matrix. Since CF and SF were mixed in the same weight ratio in this study, a large number of micro-sized fibers distributed in the specimen could be more effective for exhibiting higher heating performance than a small number of macro-sized fibers distributed in the specimen, when considering the difference in density between the two fibers.



(**a**) (**b**)

Figure 1. SEM images of CF and SF with a magnification of: (**a**) 10,000× (CF), and (**b**) 150× (SF).

2.3. Mix Proportion and Specimen Preparation

Table 4 shows the mix proportions of mortars and designations of specimens for preparing PM and ECM. Selected here was a mixing ratio of 0.44 for water to cement (W/C), and the mix proportion (weight ratio) of the materials was 0.44:1:2 water:cement:sand. Specimens of ECM were fabricated by mixing 0.25, 0.5, 0.75, 1.0 and 1.25% at 0.25% intervals in volume fractions. In order to maintain the dispersibility and workability of CF, the dosage of SP admixture added was 0.5 to 1.0% of the cement mass and, in the case of ECM mixed with SF and PM, no separate SP admixture was used.

Figure 2 displays the detailed fabrication process of each specimen step by step. As demonstrated in Figure 2a, cement, standard sand, CF or SF, water and SP admixture were weighed on the basis of Table 4. A laboratory Hobart mixer was used to prepare fresh mixtures. Cement and standard sand were dry mixed for 2 min to ensure material homogeneity (Figure 2b). As seen in Figure 2c, fibers were added and water and SP admixture were mixed for 3 min after dry mixing of cement and standard sand was completed (Figure 2d). The mortar mixture was poured into a mold and, after dividing the mixture into three layers, compaction was performed 25 times for each layer. First of all, the first layer was poured and compacted to make the mortar mixture (Figure 2e). Electrodes were embedded at 40 mm intervals after compacting the first layer to prevent fiber balls (Figure 2f). After the electrodes were embedded, the second and third layers were poured and compacted (Figure 2g). Finally, in an attempt to minimize voids within the specimen, the layers were vibrated for about 3 min using a vibrating table in the laboratory. The surfaces of the specimens were finished with a steel trowel. All specimens were demolded

after 24 h and kept in an air-dried state until right before the test to minimize the effect of the curing environment on the heating performance (Figure 2h).

Table 4. Designations of specimens and mix proportions of mortars (from 0 vol% to 1.25 vol%).

Designations	Fiber Contents by Volume				Unit (kg/m^3)			SP [1] (%)
	CF		SF		Water	Cement	Sand	
	%	kg/m^3	%	kg/m^3				
ECM-CF25	0.25	4.5						
ECM-CF50	0.50	9.0						
ECM-CF75	0.75	13.5			198	450	900	0.5~1.0
ECM-CF100	1.00	18.0						
ECM-CF125	1.25	22.5						
ECM-SF25			0.25	19.62				
ECM-SF50			0.50	39.25				
ECM-SF75			0.75	58.87	198	450	900	-
ECM-SF100			1.00	78.50				
ECM-SF125			1.25	98.12				
PM	Plain cement mortar mixture (0% conductive fiber)				198	450	900	-

[1] SP = superplasticizer (% mass of cement).

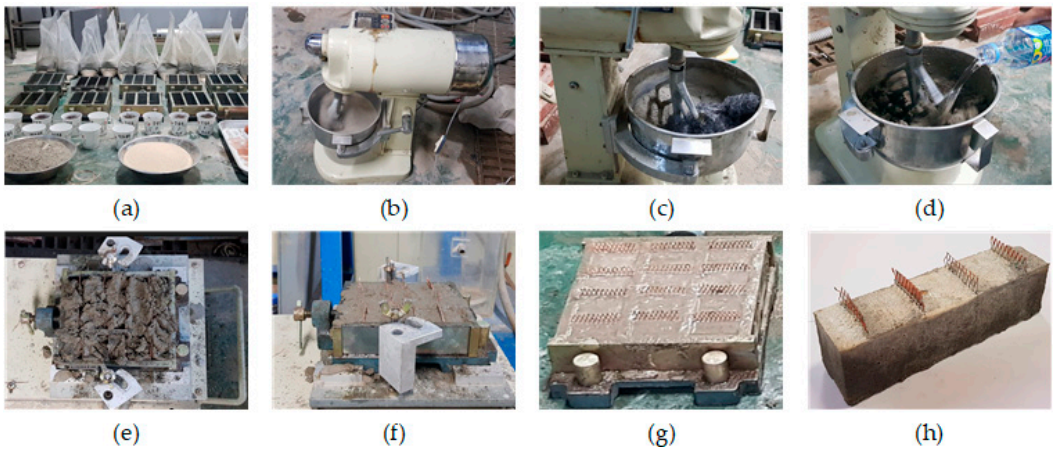


Figure 2. Fabrication process of ECM by every stage: (**a**) material preparation, (**b**) dry mixing (2 min), (**c**) fiber input, (**d**) addition of water and SP admixture (3 min), (**e**) pouring and compaction of the 1st floor, (**f**) pouring and copper mesh installation, (**g**) 2nd and 3rd floor compaction (3 min) and (**h**) demolding and curing.

2.4. Arrangement of Electrodes and Voltage Application Method

Figure 3 features the configuration of the copper mesh electrodes embedded in the specimen to apply voltage. As shown in Figure 3, the electrodes were embedded at 40 mm intervals in a straight line with four copper meshes arranged in a row at equal intervals on the prism-shaped specimens, prepared with dimensions of 40 × 40 × 160 mm. The two electrodes were installed at a distance of 40 mm and 120 mm, respectively, and a copper mesh was employed to minimize the contact resistance between the cement and the electrode. In this study, the heating performance test was performed by applying DC voltages of 10 V, 20 V and 30 V to the prismatic specimens. The DC voltage application method was divided into two cases as shown in Figure 3. In case 1, the voltage was applied by connecting the electrodes installed at the two measuring points A and D at both ends of the specimen; in case 2, the voltage was applied by connecting the electrodes installed at measuring points B and C of the specimen. In case 1, the total volume of the voltage-applicable part is 40 × 40 × 120 mm^3 while, in case 2, the total volume of the voltage-applicable part is 40 × 40 × 40 mm^3.

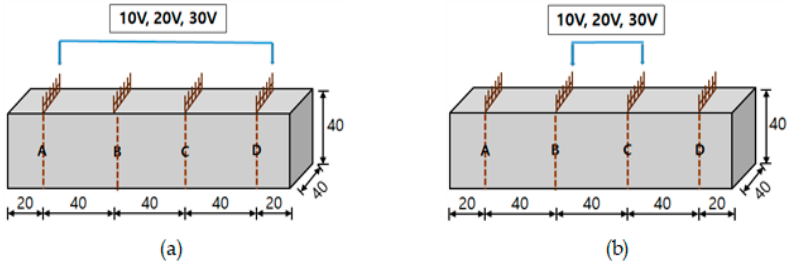


Figure 3. Cases of the applied voltages in heating performance test: (**a**) Case 1: 10 V, 20 V, 30 V applied at points A and D and (**b**) Case 2: 10 V, 20 V, 30 V applied at points B and C.

2.5. Experimental Methods

2.5.1. Heating Performance Test

There are neither separate domestic nor foreign regulations on test standards to evaluate the heating performance of cement-based composites. The voltage applied when conducting heating performance tests varies greatly among researchers. The dimensions of the specimens used in this study were fabricated to be 40 × 40 × 160 mm in accordance with KS L ISO 679 [36] and ASTM C348 [37], which are domestic and foreign standards for flexural strength tests. Clamps were connected to the (+) and (−) ends of the electrodes of the copper mesh embedded in the specimen, and then voltages of 10 V, 20 V and 30 V were applied for 3600 s using a DC power supply (AK 3005). Then, the surface temperature was measured at intervals of 10 s. The maximum output voltage and current of the power supply were 30 V and 3 A (90 VA), respectively. At the same time, the surface temperature was measured in real time through an infrared thermal camera (FLIR T630sc, Wilsonville, OR, USA). Figure 4 shows the overall schematic diagram and test setup scene for measuring the surface temperature of the specimens. The initial temperature of all specimens before applying voltage was about 20 °C, and the distance between the infrared thermal camera and the specimen was fixed at about 45 cm. In addition, the laboratory room temperature was kept constant at about 20 ± 1 °C and the humidity was set in the range of 50 ± 5% in order to prevent heat loss due to the temperature difference between the specimen and the surroundings of the laboratory. For checking the strength of the applied voltage, a multitester was used to confirm the application of constant voltage, and all specimens were placed on an insulating rubber plate and a constant voltage was applied to ensure safety by preventing electrical shock and short circuits while testing.

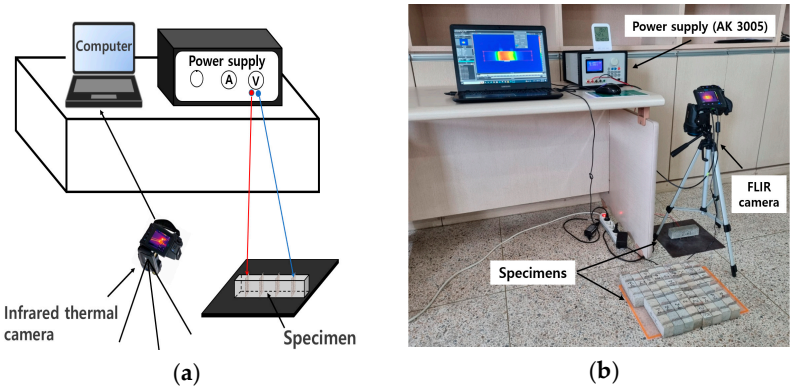


Figure 4. Surface temperature measurements via infrared thermal camera with the applied voltage: (**a**) schematic diagram, (**b**) test setup.

2.5.2. Flexural Strength Test

In the flexural strength test, the flexural strength was measured at the age of 28 ages with the molds fabricated according to the specifications KS L ISO 679 [36] and ASTM C348 [37]. The cured specimens with dimensions of 40 × 40 × 160 mm were subjected to a

three-point flexural test at a speed of 50 N/s using a universal testing machine (manufacturer: MTDI Co., Ltd., Daejeon, Republic of Korea; model name: UT-100F) with a capacity of 100 kN to measure the strength. The flexural strength was calculated as the average value of the three specimens using Equation (1).

$$f_r = 6M/bd^2 \quad (1)$$

Here, f_r is the flexural strength (MPa), M is the maximum flexural moment (N·mm), b is the width of the specimen (40 mm) and d is the depth of the specimen (40 mm).

2.5.3. SEM Observation

A SEM is a device that scans an electron beam on the surface of a sample to generate secondary electrons to observe the morphology of the microscopic sample surface. In this study, SEM images were taken to determine the fiber morphology and distribution within the cement matrix under repetitive electrical heating. The analysis equipment used TESCAN's MIRA3-LMH high-resolution field emission scanning electron microscope (FE-SEM, model name). Following the heating performance test, the cured specimens were pulverized and the obtained fiber was dried, coated with platinum in a vacuum state and then observed through a SEM.

2.5.4. TGA Analysis

In this study, we measured the weight loss according to the temperature change of the sample using a thermogravimetric analyzer (TGA) device. For the TGA analysis of the specimens prepared according to Table 4, about 3 g of sample was taken. About 10 mg of the pulverized fine powder sample was placed in an alumina cup on a platinum plate and subjected to TGA analysis. The equipment used in this study was a TGA 550 Auto from TA Instruments, USA, whose temperature can rise from 0 °C to 1000 °C. The heating rate in the test was fixed at 10 °C/min, and it was performed under a nitrogen gas environment.

3. Results and Analysis

3.1. Results of the Heating Performance Test

Table 5 summarizes the maximum heating performance test results according to the parameters of each specimen, and Figure 5 shows them in comparison. As seen in Table 5 and Figure 5, the results of measurement for 3600 s after supplying three different applied voltages (DC 10 V, 20 V, 30 V) for different electrode spacings (40 mm, 120 mm) showed that, in the case of the PM specimen, the maximum heating temperature was 20.1 °C, 20.2 °C and 20.3 °C, respectively, showing very low heating performance without apparent dependence on applied voltages or electrode spacings. Even in the case of the ECM specimens mixed with SF under the same conditions, the maximum heating temperature was slightly improved to 20.2~20.6 °C, 20.3~21.2 °C and 20.4~21.8 °C, respectively, and we could not find any distinct differences in heating performance due to the difference in electrode spacing. The heating values of the ECM specimens mixed with SF and PM specimens were at most 0.3 °C and 1.8 °C, respectively, showing very low heating performance and almost no heating effect. Therefore, because electrically conductive properties were not improved in this way, it was judged that snow and ice accumulated on the surface of the pavement could not be removed. However, the maximum heating temperature of the ECM specimens mixed with CF witnessed significant improvements in the heating performance compared to the PM specimen and the ECM specimens mixed with SF. At three different applied voltages (DC 10 V, 20 V, 30 V) and different electrode spacings (40 mm, 120 mm), the maximum heating temperatures increased greatly to 20.6~34.8 °C, 24.9~73.7 °C and 30.1~145.1 °C, respectively. As the CF contents and applied voltages increased, the maximum heating temperature tended to increase. In particular, the highest heating temperature occurred in the ECM-CF125 specimen mixed with CF, with applied voltage of 30 V and electrode spacing of 40 mm, reaching a maximum of 145.1 °C. The reason for such better heating performance is that the CF in the specimen contact each

other to form more electrically conductive networks through which electricity can flow easily. This is known from previous research results also stating the enhanced heating performance effect [38]. It is expected that this generated heat can be effectively used to melt snow and ice accumulated on the surface of the pavements.

Table 5. The results of maximum heating temperature measurements for the specimens.

Designations	Fiber Type	Fiber Contents (%)	Maximum Heating Temperatures (°C)					
			10 V		20 V		30 V	
			120 mm	40 mm	120 mm	40 mm	120 mm	40 mm
ECM-CF25	CF	0.25	20.6	21.8	24.9	34.3	30.1	77.0
ECM-CF50		0.50	20.7	22.3	27.0	37.5	31.3	79.6
ECM-CF75		0.75	21.3	25.4	40.9	48.4	42.6	88.1
ECM-CF100		1.00	23.4	27.7	41.1	51.4	54.8	140.5
ECM-CF125		1.25	23.3	34.8	46.5	73.7	65.9	145.1
ECM-SF25	SF	0.25	20.2	20.2	20.3	20.3	20.4	20.4
ECM-SF50		0.50	20.2	20.2	20.3	20.3	20.5	20.5
ECM-SF75		0.75	20.3	20.3	20.5	20.6	20.8	20.9
ECM-SF100		1.00	20.4	20.5	20.7	20.8	21.1	21.3
ECM-SF125		1.25	20.5	20.6	21.0	21.2	21.5	21.8
PM	-	-	20.1	20.1	20.2	20.2	20.3	20.3

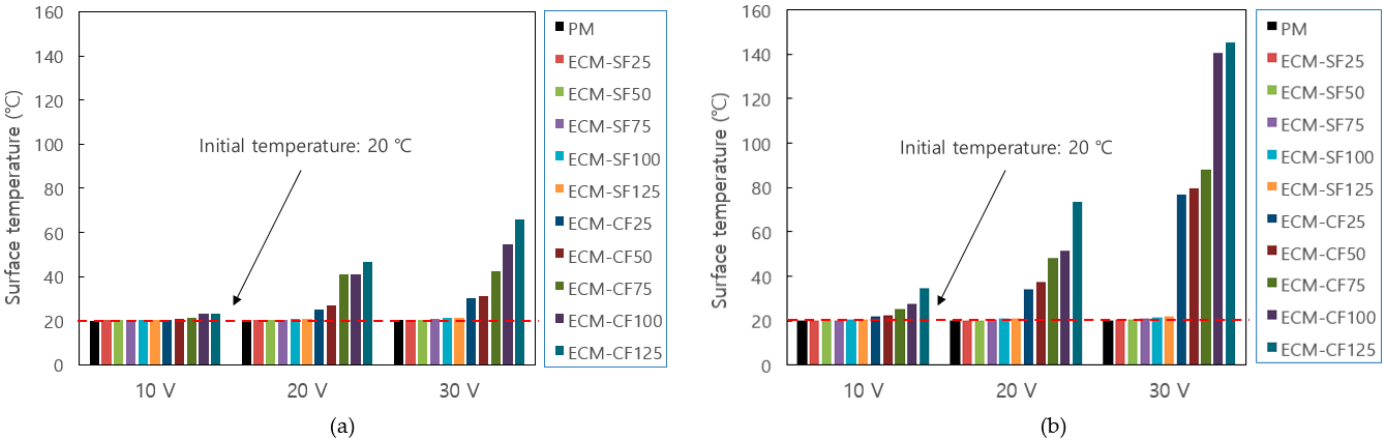


Figure 5. Maximum heating temperatures of ECM specimens and PM specimen according to applied voltages: (**a**) 120 mm, and (**b**) 40 mm.

3.2. Temperature Variation Curves during the Elapsed Time

Figure 6 is a group of graphs showing the surface temperature variation curves during the elapsed time of experimentation for ECM specimens mixed with SF compared to the PM specimen. As shown in Figure 6, each graph shows a constant trend with little variation in temperature compared to the initial temperature. In the case of the PM specimen as seen in Figure 6 and Table 5, the surface temperature reached 20.1 °C, 20.2 °C and 20.3 °C after 3600 s at applied voltages of 10 V, 20 V and 30 V, respectively. Regardless of the electrode spacing, an increase of 0.1~0.3 °C compared to the initial temperature (20 °C) was found, which indicates little temperature variation. In addition, even in the case of the ECM specimens mixed with SF as shown in Figure 6 and Table 5, for the same three applied voltages, the surface temperatures reached 20.2~20.6 °C, 20.3~21.2 °C and 20.4~21.8 °C, respectively, which represented increases of 0.2~0.6 °C, 0.3~1.2 °C and

0.4~1.8 °C, respectively, compared to the initial temperature. The heating value was so insignificant that the surface temperature was similar to the ambient temperature. On the other hand, Figure 7 features graphs showing the surface temperature variation curves during the elapsed time of experimentation for ECM specimens mixed with CF compared to the PM specimen. In all graphs except for Figure 7a, the surface temperature increased gradually from the initial stage, showing a tendency of convergence to a certain value after reaching the maximum point. As shown in Figure 7a, the surface temperature of specimens reached 20.6~23.3 °C at an applied voltage of 10 V and an electrode spacing of 120 mm, which is an increase by 0.6~3.3 °C compared to the initial temperature, indicating that there was almost no temperature variation. According to Figure 7b, however, the surface temperature of specimens reached 21.8~34.8 °C at an applied voltage of 10 V and an electrode spacing of 40 mm, a 1.8~14.8 °C increase compared to the initial temperature. Figure 7c shows that the surface temperature of specimens reached 24.9~46.5 °C even at an applied voltage of 20 V and an electrode spacing of 120 mm, a 4.9~26.5 °C increase compared to the initial temperature, while Figure 7d reveals that the surface temperature of specimens reached 34.3~73.7 °C at an applied voltage of 20 V and an electrode spacing of 40 mm, a significant 14.3~53.7 °C increase compared to the initial temperature. As shown in Figure 7e, the surface temperature of specimens reaches 30.1~65.9 °C at an applied voltage of 30 V and the electrode spacing of 120 mm, a significant 10.1~45.9 °C increase compared to the initial temperature. As shown in Figure 7f, the surface temperature of specimens reaches 77.0~145.1 °C at an applied voltage of 30 V and an electrode spacing of 40 mm, a 57.0~125.1 °C increased compared to the initial temperature. In particular, the most remarkable increase occurred with 145.1 °C in the ECM-CF125 specimen mixed with 1.25% CF. Such an increase in heating performance (by about 7.3 times compared to the initial temperature) seems to be related to the electrical conductivity, because it is proportional to temperature. It was determined that the heating performance of the ECM specimens mixed with CF improved as the applied voltages and fiber contents increased. The surface temperature of all specimens increased rapidly up to 20 min, then slowed down but gradually increased thereafter. In all specimens, it was confirmed that the temperature increase was similar for 40 min, and it was found that heating at 77 °C or higher was possible. This is in accordance with previous research results [38].

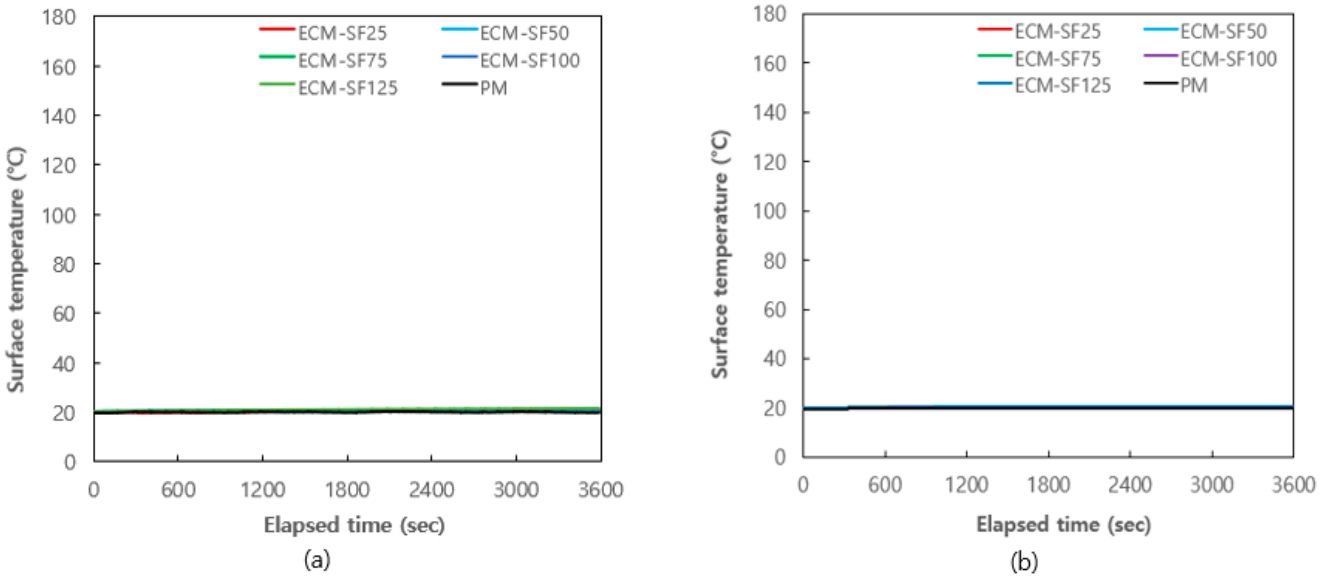


Figure 6. *Cont.*

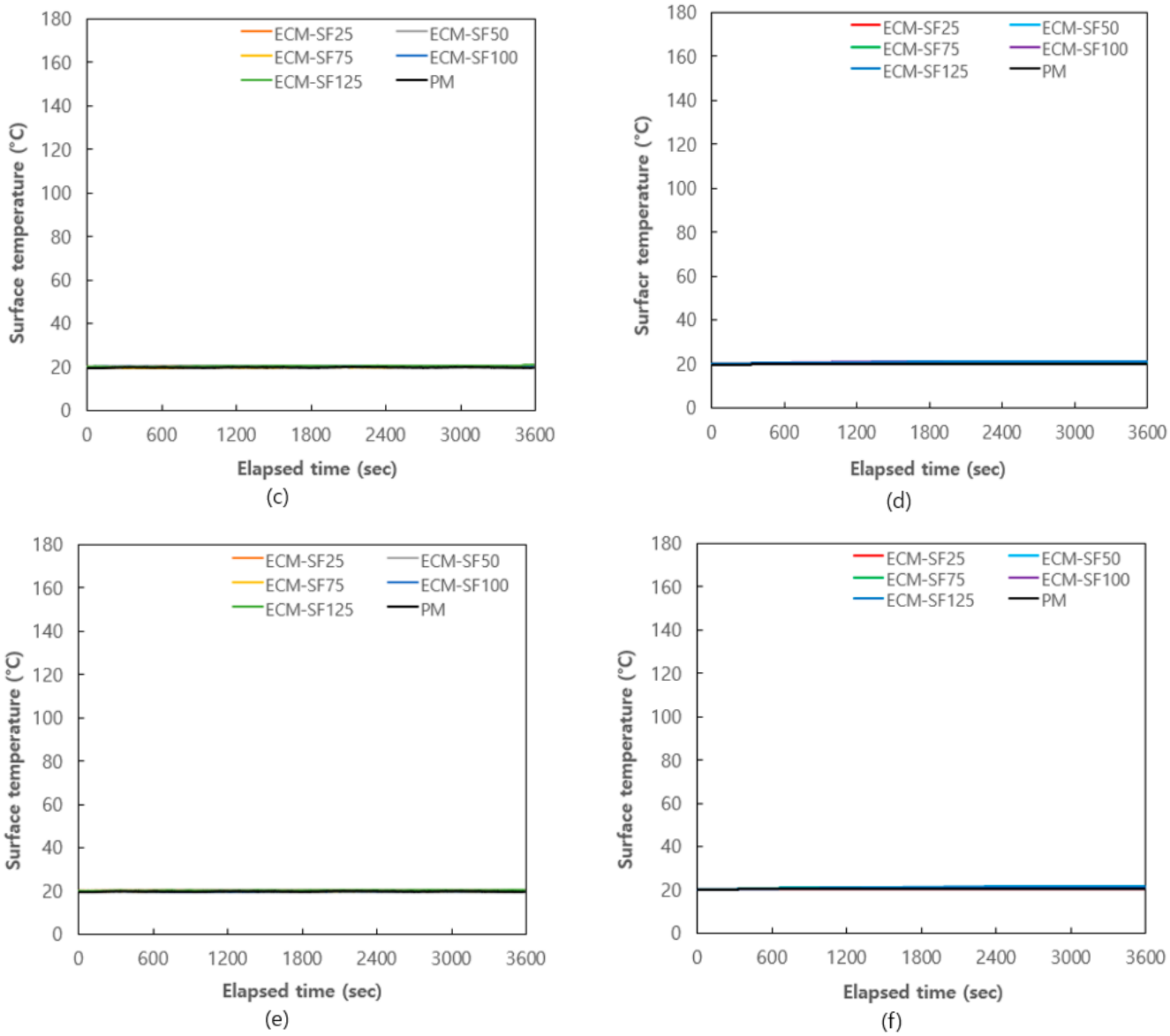


Figure 6. Temperature variation of ECM specimens mixed with SF vs PM specimen: (**a**) 10 V and 120 mm, (**b**) 10 V and 40 mm, (**c**) 20 V and 120 mm, (**d**) 20 V and 40 mm, (**e**) 30 V and 120 mm and (**f**) 30 V and 40 mm.

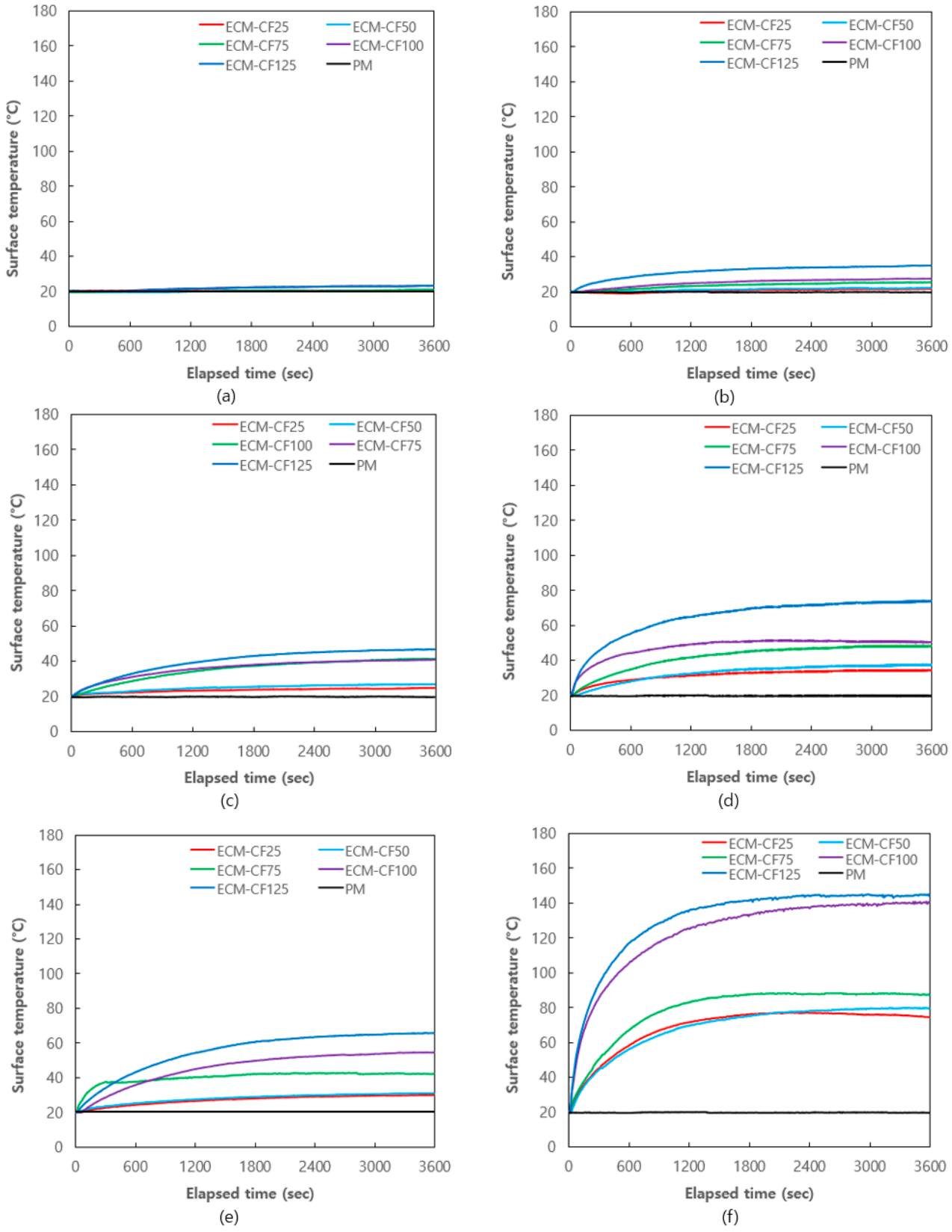


Figure 7. Temperature variation of ECM specimens mixed with CF vs PM specimen: (**a**) 10 V and 120 mm, (**b**) 10 V and 40 mm, (**c**) 20 V and 120 mm, (**d**) 20 V and 40 mm, (**e**) 30 V and 120 mm and (**f**) 30 V and 40 mm.

3.3. Infrared Thermal Image Analysis

In this study, the surface temperature of specimens was photographed using an infrared thermal camera (FLIR T630sc, Wilsonville, OR, USA) to check the heat distribution and temperature transfer pattern of PM and ECM specimens. The initial temperature of specimens is about 20 °C, and the surface temperature of specimens is marked on the infrared thermal images together with the initial temperature. Figure 8 shows infrared thermal images according to the parameters of each specimen taken at an applied voltage of 30 V and an electrode spacing of 120 mm. As seen in Figure 8a, the surface temperature of the PM specimen was measured to be 20.3 °C. As it was similar to the ambient room temperature, it was impossible to distinguish a clear difference in heating performance depending on the applied voltage. As shown in Figure 8b–d, the surface temperature of ECM specimens mixed with SF slightly increased to 20.4~21.5 °C, and the amount of heat generated was very insignificant, so the infrared thermal images were not clear. Because of this, heat could not be diffused throughout the specimen. In Figure 8e–i, however, the surface temperature of ECM specimens mixed with CF was measured at 30.1~65.9 °C, indicating that the temperature increases as the heat is diffused widely to the surroundings. It was confirmed through the infrared thermal images that the heating performance improved as the CF content increased.

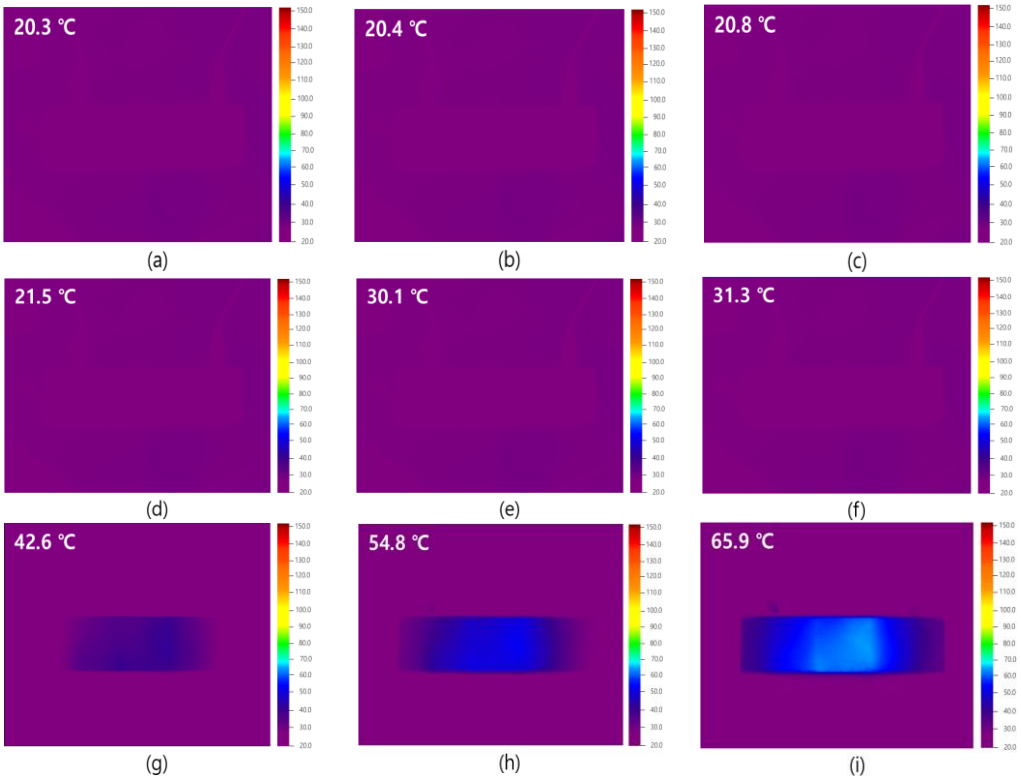


Figure 8. Surface temperature distribution in the ECM captured by an infrared thermal camera at 30 V and 120 mm: (**a**) PM, (**b**) ECM-SF25, (**c**) ECM-SF75, (**d**) ECM-SF125, (**e**) ECM-CF25, (**f**) ECM-CF50, (**g**) ECM-CF75, (**h**) ECM-CF100, (**i**) ECM-CF125.

On the other hand, Figure 9 shows infrared thermal images according to the parameters of each specimen taken at an applied voltage of 30 V and an electrode spacing of 40 mm. As shown in Figure 9a–d, the surface temperature of the PM specimen and the ECM specimens mixed with SF was slightly improved to 20.3~21.8 °C, and the amount of heat generated was very insignificant, so the infrared thermal image was not clear. As evidenced in Figure 9e–g, however, the surface temperature of the ECM specimens mixed with CF was measured to be 77.0~88.1 °C, which was a significant improvement, and it was, thus, confirmed

that the heat was distributed throughout and transferred to the specimen subsequently. In particular, from Figure 9h,i, it was confirmed that the heating performance improved greatly as the CF content increased. The highest surface temperature was 145.1 °C, which occurred in the ECM-CF125 specimen with 1.25% of mixed CF with an applied voltage of 30 V and an electrode spacing of 40 mm. The surface temperature of the specimen improved as the CF content increased, and the infrared thermal images became sharper and clearer. From the infrared thermal images, it was made clear that the heating performance was significantly improved. The analysis of the infrared thermal images revealed that the generated heat occurred mainly between the electrodes connected to the power supply, and the narrower the electrode spacing, the more advantageous it was in securing the heating performance. Such a result is believed to be due to heat diffusion and temperature transfer between the electrodes, the shortest distance, because current has a property of flowing across the shortest distance. Our results are in accordance with previous research results [39].

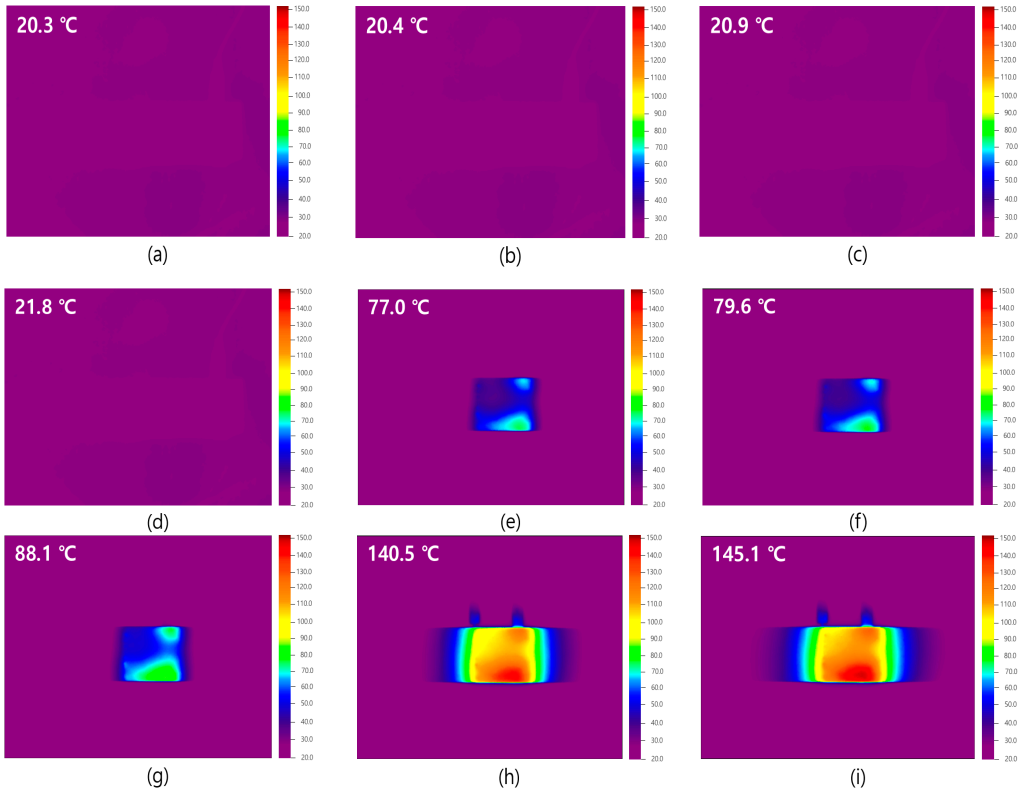


Figure 9. Surface temperature distribution in the ECM captured by an infrared thermal camera at 30 V and 40 mm: (**a**) PM, (**b**) ECM-SF25, (**c**) ECM-SF75, (**d**) ECM-SF125, (**e**) ECM-CF25, (**f**) ECM-CF50, (**g**) ECM-CF75, (**h**) ECM-CF100, (**i**) ECM-CF125.

3.4. Analysis of Flexural Strength

In road pavement, flexural strength is the most basic variable in identifying material properties and is a factor for measuring strength. In road pavement, compressive strength performance and flexural strength performance are the most basic factors in determining the physical properties of materials. It is well known that cement-based composites have excellent compressive strength but are very weak in flexural strength and have low deformability. In this study, as indicated in Table 4, in order to measure the flexural strength of the ECM under the same mixing conditions, the fiber contents were changed by 0.25% to 0.25, 0.5, 0.75, 1.0 and 1.25% in volume fractions to prepare specimens. Figure 10 features a graph showing the average flexural strength measurement results according to the fiber contents of ECM mixed with CF and SF compared to PM. In Figure 10, the average flexural

strength of PM was measured to be 3.76 MPa, and as the contents of CF increased, the flexural strength did not always increase but increased and thereafter decreased. When CF was overused, it was difficult to disperse evenly within the cement matrix and became bundled, resulting in a decrease in flexural strength. In particular, in the case of the ECM-CF125 specimen mixed with 1.25% CF, the flexural strength decreased rapidly. This signifies that when a large amount of CF is mixed, this causes a decrease in flexural strength because the dispersibility and workability are not good due to the fiber balling phenomenon. Multiple repeated mixing introduces a large number of air bubbles and may create many pores within the cement matrix. These findings have also been reported in previous studies [40]. The average flexural strength of all specimens except for the PM and ECM-CF125 specimen mixed with CF was 4.5 MPa or more, and it turned out to satisfy the flexural strength requirements currently applied in the standard specifications for road construction in the Republic of Korea. On the other hand, SF demonstrated an excellent effect on improving the flexural strength, and the average flexural strength of the ECM-SF125 specimen mixed with SF was improved by about 96% or more compared to the PM specimen. It is believed that this is because, as the content of SF increases, it acts as a bridging effect between the fiber and the matrix to prevent crack propagation and improves the flexural strength through the redistribution of stress. However, as the content of SF increased, the flexural strength significantly improved, but when 1.25% was mixed, the dispersibility of the fibers decreased due to fiber balling, and it tended to decrease slightly. In addition, in self-heating cement-based composites, microcracks may occur due to a difference in temperature between the inside and the outside owing to heat generation, and such microcracks can reduce the heating performance. It is, thus, believed that the incorporation of SF enhances the durability of cement-based composites because it has the effect of preventing microcracks in addition to the effect of increasing the flexural strength. Figure 11 shows the increase rate of the flexural strength of ECM-CF and ECM-SF specimens in comparison to the PM specimen.

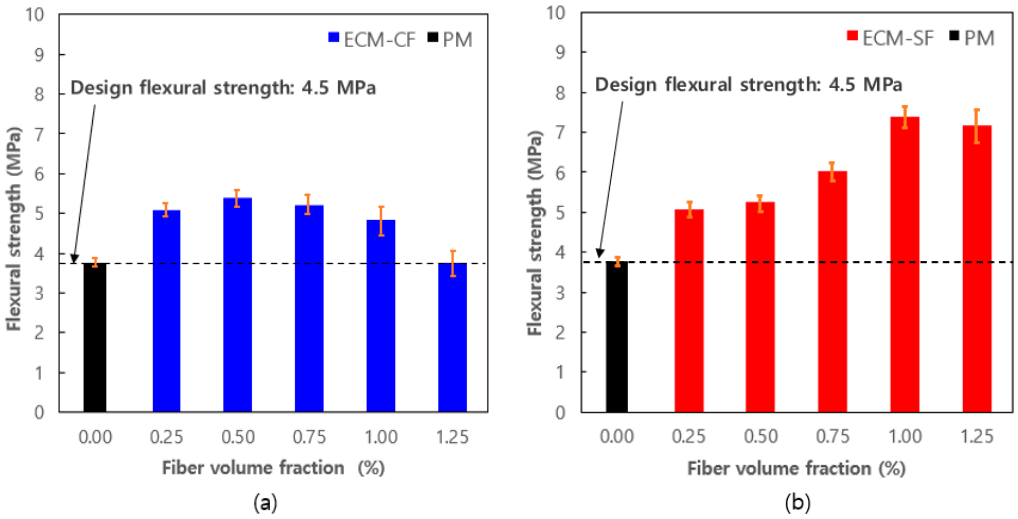


Figure 10. The effect of fiber contents on the flexural strength of ECM compared to PM: (**a**) ECM-CF vs. PM, and (**b**) ECM-SF vs. PM.

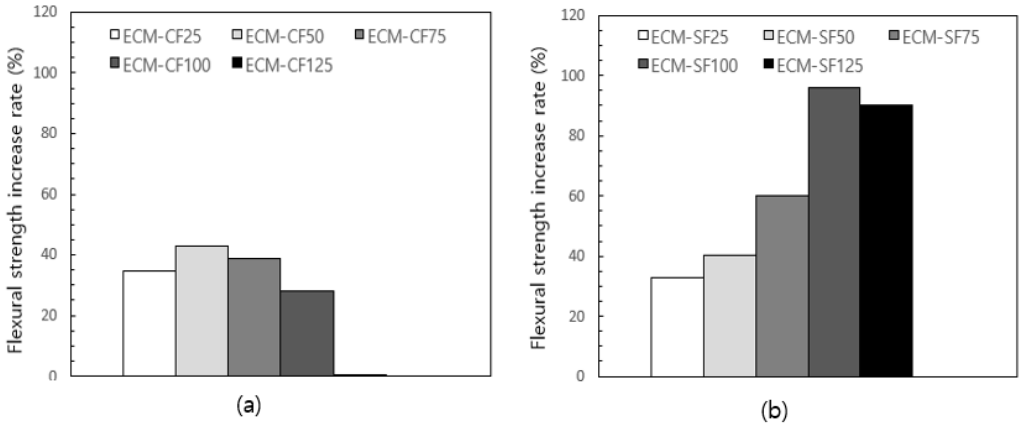
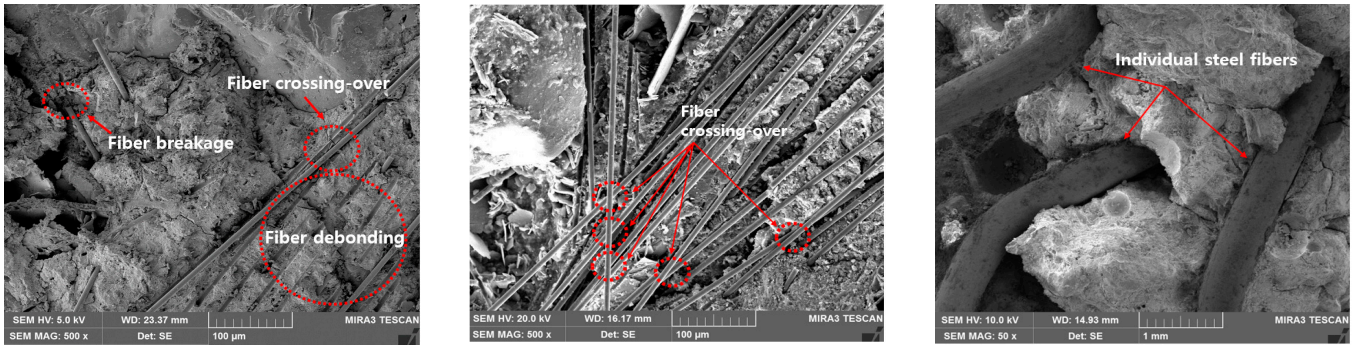


Figure 11. Percentage increase in flexural strength of ECM compared to PM: (**a**) ECM-CF vs. PM and (**b**) ECM-SF vs. PM.

3.5. SEM Analysis

In this study, SEM image analysis was performed to observe the fiber morphology and dispersion in ECM specimens mixed with CF and SF under repetitive electrical heating. Figure 12 displays SEM images of the ECM specimens mixed with CF. As shown in Figure 12a, CF within the cement matrix forms an electrical pathway that acts as a bridging among the pores. It is believed that an electrically conductive network formed in this way serves as a passage through which electrons flow, thereby improving heat generation performance. From Figure 12b, however, we can see the fiber balling of CF which has the property of hydrophobicity in the formed ECM. When mixing the mortar, such fiber balls occur frequently due to the high aspect ratio of CF, and CF that is not evenly distributed due to fiber balling happens to act as some voids. This phenomenon often occurs as the CF content increases, thus negatively affecting the improvement in flexural strength. On the other hand, Figure 12c shows SEM images of the ECM specimens mixed with SF. In Figure 12c, however, even when mixed up to 1.25%, the heating performance was not improved because an electrically conductive network was not formed within the ECM-SF125 specimen. As a result, it is judged that the incorporation of SF has little effect on the heating performance of the ECM.



(**a**) (**b**) (**c**)

Figure 12. SEM images of specimens for 1.25% carbon fiber and 1.25% steel fiber: (**a**) ECM-CF (500×), (**b**) ECM-CF (100×) and (**c**) ECM-SF (50×).

3.6. TGA Analysis

TGA analysis is a way to continuously measure and analyze the weight change of a specimen while heating it at a constant temperature increase rate. TGA curves can be graphed, and the temperature at which components are decomposed by heat can be analyzed. Cement-based composites contain many hydration products by the hydration

reaction of cement, and these hydration products change their crystal structure according to the change in temperature and absorb or release energy when they change. According to previous studies, cement-based composites release free pore water and gel water at 100 °C or higher with respect to heat and are chemically deteriorated at 300 °C or higher. Within the range of about 450 to 550 °C, calcium hydroxide ($Ca(OH)_2$), the main component of cement, is decomposed by heat, and then dehydration is accelerated, and at about 600 to 700 °C or higher, calcium carbonate ($CaCO_3$) is decomposed. It is known that complete dehydration and decomposition of cement paste finally occur above 700 °C [41,42]. In this study, the change in thermal weight was observed while increasing the temperature range of PM and ECM samples from 20 °C to 980 °C. Figure 13 is a graph showing the thermogravimetric analysis of the specimens before and after the heating performance test. As seen in Figure 13, the weight loss of the PM samples and the ECM samples is a slight decrease in the weight of the samples due to the evaporation of free pore water within the temperature range from 65 °C to 250 °C, but the weight loss tended to increase significantly as the temperature rose from 250 °C to 700 °C. It became obvious that calcium hydroxide ($Ca(OH)_2$) and calcium carbonate ($CaCO_3$) which are major hydration products within the cement matrix were decomposed by heat, resulting in a rapid decrease in the samples' weight. Finally, when the temperature of the samples becomes higher than 700 °C, one can find that the cement paste experiences complete decomposition and the weight loss does not increase significantly. Furthermore, the increase from 700 °C to 980 °C shows a tendency to decrease the amount of loss compared to the case of rising from 250 °C to 700 °C. In the case of ECM mixed with SF, however, there is a tendency for the temperature to rise slightly after a rapid drop to 750 °C. This is thought to be the result of the debonding and oxidation of SF. As a result of dehydration of calcium hydroxide ($Ca(OH)_2$) and decarboxylation of calcium carbonate ($CaCO_3$), in Figure 13, it can be seen that the phase change of the cement hydration products before and after the heating performance test was not significant.

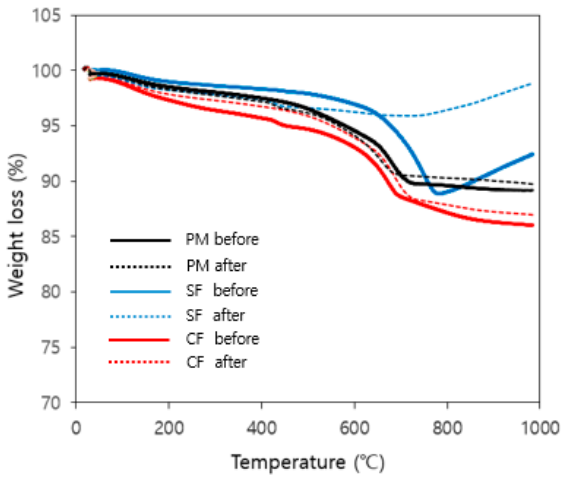


Figure 13. Results of weight analysis for samples by TGA.

4. Conclusions

In this study, ECM mixed with conductive fibers CF and SF was prepared, and its heating performance, microstructures and flexural strength properties were analyzed. The results were also compared and reviewed with PM. The conclusions drawn from this study may be summed up as follows:

1. The heating performance of ECM specimens mixed with CF tended to increase as the fiber contents and applied voltages increased. It was evident that the ECM specimens mixed with CF secured higher heating performances than the PM specimen and the ECM specimens mixed with SF. Particularly, the ECM-CF125 specimen in which 1.25% of CF was mixed showed the highest heating performance, which increased by about 7.3 times compared to the initial temperature (20 °C);

2. The infrared thermal images made it clear that the heat was distributed and the temperature was transferred depending on the parameters of each specimen. The infrared thermal images became sharper and clearer as the heating performance increased; the heating performance could be confirmed even with the naked eye;
3. The flexural strength of ECM was significantly improved as the contents of CF and SF increased. However, the flexural strength of the ECM-CF125 specimen was significantly reduced due to fiber balling. Considering that a certain level of flexural strength is required in order to use ECM mixed with CF, it is determined that the use of ECM mixed with up to 1.0% of CF is most appropriate;
4. From the result of images analysis using SEM, it was confirmed that the CF formed an electrically conductive network and, in some cases, fiber clumping and balling were observed following the heterogeneous dispersion of CF. Such fiber clumping and balling phenomena of CF cause a decrease in flexural strength;
5. Although there was a slight difference in the amount of thermal weight loss for the samples before and after the heating performance test, it was confirmed that the ECM samples were relatively unchanged even under repetitive electrical heating.

Author Contributions: Conceptualization, D.-J.S. and J.-G.P.; methodology, D.-J.S. and J.-G.P.; validation, G.-H.H. and Y.-J.L.; formal analysis, B.-G.C. and J.-G.P.; investigation, J.-G.P., D.-J.S. and Y.-J.L.; writing—original draft preparation, D.-J.S. and J.-G.P.; writing—review and editing, G.-H.H. and D.-J.S.; visualization, J.-G.P., Y.-J.L. and B.-G.C.; supervision, G.-H.H.; project administration, G.-H.H.; funding acquisition, G.-H.H. All authors have read and agreed to the published version of the manuscript.

Funding: This research was funded by the Basic Science Research Program through the National Research Foundation of Korea (NRF) of the Ministry of Education, Republic of Korea (Grant no. NRF-2018R1A6A1A03025542).

Institutional Review Board Statement: Not applicable.

Informed Consent Statement: Not applicable.

Data Availability Statement: Not applicable.

Conflicts of Interest: The authors declare no conflict of interest.

References

1. Chung, D.D.L. Cement reinforced with short carbon fibers: A multifunctional material. *Compos. Part B Eng.* **2000**, *31*, 511–526. [CrossRef]
2. El-Dieb, A.S.; El-Ghareeb, M.A.; Abdel-Rahman, M.A.H.; Nasr, E.S.A. Multifunctional electrically conductive concrete using different fillers. *J. Build. Eng.* **2018**, *15*, 61–69. [CrossRef]
3. Saraireh, D.; Suryanto, B.; McCarter, W.J.; Walls, S. The electro-mechanical tensile properties of an engineered cementitious composite. *Adv. Cem. Res.* **2021**, *33*, 478–495. [CrossRef]
4. Catalá, G.; Ramos-Fernández, E.V.; Zornoza, E.; Andión, L.G.; Garcés, P. Influence of the oxidation process of carbon materials on the mechanical properties of cement mortars. *J. Mater. Civil. Eng.* **2011**, *23*, 321–329. [CrossRef]
5. Gomis, J.; Galao, O.; Gomis, V.; Zornoza, E.; Garcés, P. Self-heating and deicing conductive cement. Experimental study and modeling. *Constr. Build. Mater.* **2015**, *75*, 442–449. [CrossRef]
6. Chung, D.D.L. Self-heating structural materials. *Smart Mater. Struct.* **2004**, *13*, 562–565. [CrossRef]
7. Gwon, S.W.; Moon, J.H.; Shin, M.S. Self-heating capacity of electrically conductive cement composites: Effects of curing conditions. *Constr. Build. Mater.* **2022**, *353*, 129087. [CrossRef]
8. Suryanto, B.; Wilson, S.A.; McCarter, W.J.; Chrisp, T.M. Self-healing performance of engineered cementitious composites under natural environmental exposure. *Adv. Cem. Res.* **2016**, *28*, 211–220. [CrossRef]
9. Wu, J.; Lui, J.; Yang, F. Three-phase composite conductive concrete for pavement deicing. *Constr. Build. Mater.* **2015**, *75*, 129–135. [CrossRef]
10. Malchiodi, B.; Marchetti, R.; Barbieri, L.; Pozzi, P. Recovery of cork manufacturing waste within mortar and polyurethane: Feasibility of use and physical, mechanical, thermal insulating properties of the final green composite construction materials. *Appl. Sci.* **2022**, *12*, 3844. [CrossRef]

11. Nili, M.; Afroughsabet, V. The long-term compressive strength and durability properties of silica fume fiber-reinforced concrete. *Mater. Sci. Eng. A* **2012**, *531*, 107–111. [CrossRef]
12. Kang, S.H. Electrically conductive concrete. *J. Korea Concr. Inst.* **1998**, *10*, 34–40.
13. Whittington, H.W.; McCarter, J.; Forde, M.C. The conduction of electricity through concrete. *Mag. Concr. Res.* **1981**, *33*, 48–60. [CrossRef]
14. Galao, O.; Baeza, F.J.; Zornoza, E.; Garces, P. Self-heating function of carbon nanofiber cement pastes. *Mater. Constr.* **2014**, *64*, e015.
15. Pérez, A.; Climent, M.A.; Garcés, P. Electrochemical extraction of chlorides from reinforced concrete using a conductive cement paste as the anode. *Corros. Sci.* **2010**, *52*, 1576–1581. [CrossRef]
16. Zhao, R.H.; Tuan, C.Y.; Fan, D.; Xu, A.; Luo, B. Ionically conductive mortar for electrical heating. *ACI Mater. J.* **2017**, *114*, 923–934. [CrossRef]
17. Zhao, R.H.; Tuan, C.Y.; Xu, A.; Fan, D.B. Conductivity of ionically-conductive mortar under repetitive electrical heating. *Constr. Build. Mater.* **2018**, *173*, 730–739. [CrossRef]
18. Tuan, C.Y.; Yehia, S. Evaluation of electrically conductive concrete containing carbon products for deicing. *ACI Mater. J.* **2004**, *101*, 287–293.
19. Tuan, C.Y. Roca Spur bridge: The implementation of an innovative deicing technology. *J. Cold Reg. Eng.* **2008**, *22*, 1–15. [CrossRef]
20. Wang, S.; Wen, S.; Chung, D.D.L. Resistance heating using electrically conductive cements. *Adv. Cem. Res.* **2004**, *16*, 161–166. [CrossRef]
21. Zhang, G.H.; Zhao, C.Y. Thermal and rheological properties of microencapsulated phase change materials. *Renew. Energy* **2011**, *36*, 2959–2966. [CrossRef]
22. Belli, A.; Mobili, A.; Bellezze, T.; Tittarelli, F. Commercial and recycled carbon/steel fibers for fiber-reinforced cement mortars with high electrical conductivity. *Cem. Concr. Compos.* **2020**, *109*, 103569. [CrossRef]
23. Dehghani, A.; Aslani, F. The effect of shape memory alloy, steel, and carbon fibres on fresh, mechanical, an d electrical properties of self-compacting cementitious composites. *Cem. Concr. Compos.* **2020**, *112*, 103659. [CrossRef]
24. Hembach, M.; Möller, H.; Neumann, T.; Volkmer, D. Carbon fibre reinforced cement-based composites as smart floor heating materials. *Compos. Part B Eng.* **2016**, *90*, 465–470. [CrossRef]
25. Tuan, C.Y. Electrical resistance heating of conductive concrete containing steel fibers and shavings. *ACI Mater. J.* **2004**, *101*, 65–71.
26. Sassani, A.; Arabzadeh, A.; Ceylan, H.; Kim, S.H.; Sajed Sadati, S.M.; Gopalakrishnan, K.; Taylor, P.C.; Abdualla, H. Carbon fiber-based electrically conductive concrete for salt-free deicing of pavements. *J. Clean. Prod.* **2018**, *203*, 799–809. [CrossRef]
27. Malakooti, A.; Theh, W.H.; Sajed Sadati, S.M.; Ceylan, H.; Kim, S.H.; Mina, M.; Cetin, K.; Taylor, P.C. Design and Full-scale Implementation of the Largest Operational Electrically Conductive Concrete Heated Pavement System. *Constr. Build. Mater.* **2020**, *255*, 119229. [CrossRef]
28. Mingqing, S.; Xinying, M.; Xiaoying, W.; Zuofu, H.; Zhuoqiu, L. Experimental studies on the indoor electrical floor heating system with carbon black mortar slabs. *Energy. Build.* **2008**, *40*, 1094–1100. [CrossRef]
29. Sassani, A.; Ceylan, H.; Kim, S.H.; Arabzadeh, A.; Taylor, P.C.; Gopalakrishnan, K. Development of carbon fiber-modified electrically conductive concrete for implementation in Des Moines International Airport. *Case Stud. Constr. Mater.* **2018**, *8*, 277–291. [CrossRef]
30. Tuan, C.Y.; Yehia, S. Implementation of conductive concrete overlay for bridge deck deicing at Roca, Nebraska. In Proceedings of the Sixth International Symposium on Snow Removal and Ice Control Technology, Spokane, WA, USA, 7–9 June 2004; pp. 363–378.
31. Yehia, S.; Tuan, C.Y. Conductive concrete overlay for bridge deck deicing. *ACI Mater. J.* **1999**, *96*, 382–390.
32. You, I.H.; Lee, S.J.; Zi, G.S.; Lim, D.H. Influence of carbon fiber incorporation on electrical conductivity of cement composites. *Appl. Sci.* **2020**, *10*, 8993. [CrossRef]
33. Galao, O.; Bañón, L.; Baeza, F.; Carmona, J.; Garcés, P. Highly conductive carbon fiber reinforced concrete for icing prevention and curing. *Materials* **2016**, *9*, 281. [CrossRef] [PubMed]
34. Chen, B.; Wu, K.; Yao, W. Conductivity of carbon fiber reinforced cement-based composites. *Cem. Concr. Compos.* **2004**, *26*, 291–297. [CrossRef]
35. *Ministry of Land, Infrastructure and Transport*; Road Construction Standard Specification: Sejong, Republic of Korea, 2016.
36. *KS L ISO 679*; Methods of Testing Cements-Determination of Strength. Korean Agency for Technology and Standards (KATS): Eumseong County, Republic of Korea, 2016.
37. *ASTM C348*; Standard Test Method for Flexural Strength of Hydraulic-Cement Mortars. American Society for Testing Materials (ASTM) International: West Conshohocken, PA, USA, 2009.
38. Jang, D.I.; Yoon, H.N.; Yang, B.J.; Khalid, H.R.; Walls, S. Cyclic heat-generation and storage capabilities of self-heating cementitious composite with and addition of phase material. *Constr. Build. Mater.* **2023**, *369*, 130512. [CrossRef]
39. Park, S.H.; Lee, H.Y.; Chung, W.S. Experimental study on voltage supply efficiency of nano cement composites for prevention of road icing. *J. Korean Soc. Hazard Mitig.* **2018**, *18*, 221–228. [CrossRef]
40. Heo, G.H.; Park, J.G.; Song, K.C.; Park, J.H.; Jun, H.M. Mechanical properties of SiO_2-coated carbon fiber-reinforced mortar composites with different fiber length and fiber volume fractions. *Adv. Civ. Eng.* **2020**, *2020*, 8881273. [CrossRef]

41. Won, J.P.; Park, K.H.; Park, C.G. Performance of hybrid reinforced concrete at elevated high temperature. *J. Korea Concr. Inst.* **2008**, *20*, 325–333.
42. Liu, Y.; Wang, M.; Tian, W.; Qi, B.; Lei, Z.; Wang, W. Ohmic heating curing of carbon fiber/carbon nanofiber synergistically strengthening cement-based composites as repair/reinforcement materials used in ultra-low temperature environment. *Compos. Part A Appl. Sci. Manuf.* **2019**, *125*, 105570. [CrossRef]

Disclaimer/Publisher's Note: The statements, opinions and data contained in all publications are solely those of the individual author(s) and contributor(s) and not of MDPI and/or the editor(s). MDPI and/or the editor(s) disclaim responsibility for any injury to people or property resulting from any ideas, methods, instructions or products referred to in the content.